

Elastic scattering and breakup effect analysis of $^{11}\text{Be} + ^{12}\text{C}$ at 38.4 MeV/nucleon

M. Y. M. Hassan,^{1,*} M. Y. H. Farag,^{1,†} E. H. Esmail,¹ and H. M. Maridi^{1,2,‡}

¹Physics Department, Faculty of Science, Cairo University, Cairo, Egypt

²National Atomic Energy Commission, Sana'a, Yemen

(Received 16 April 2009; published 18 June 2009)

$^{11}\text{Be} + ^{12}\text{C}$ elastic-scattering data at 38.4 MeV/nucleon has been analyzed using the optical model. The optical potential is calculated in the framework of the double folding model using M3Y effective nucleon-nucleon interaction. Different models of ^{11}Be density are tested and the model that does not include the halo structure gives poor fitting with data. The breakup effect is studied by introducing a complex dynamical polarization potential (DPP) that is added to the “bare” potential. The DPP is taken in different forms that have been obtained from simple phenomenological, semiclassical approximation, and microscopic methods. The simple phenomenological DPP is related to the semiclassical approximation method. The sensitivity of the differential and reaction cross sections to these polarization potentials is tested. The microscopic DPP that has been constructed from the derivative of the folding potential describes the breakup effect well. It gives an explicit justification for the long range of the polarization potential.

DOI: [10.1103/PhysRevC.79.064608](https://doi.org/10.1103/PhysRevC.79.064608)

PACS number(s): 21.10.Gv, 24.10.Ht, 25.60.Bx

I. INTRODUCTION

Light neutron-rich exotic nuclei are characterized by weak binding energies that lead to “exotic” features such as halos [1]. The striking feature of the halo nuclei is the long tail of their matter density due to their weak binding energy, so the probability to be excited to continuum states is higher compared to the stable isotopes. Also, the coupling to the other reaction processes may be stronger [2]. The optical potential is the basic part for description of the elastic scattering, and it is also important in breakup calculations.

The interaction potential arising from coupling to nonelastic channels is called the dynamical polarization potential (DPP) [3]. It is weak but has a longer range than the “bare” optical potential, and it is complex with repulsive real part [4,5]. There are several models to obtain DPP that represents the effect of the breakup of halo nuclei and it is added to “bare” halo-target optical potential. It is stimulated by a complex phenomenological surface Woods-Saxon (WS) potential [2,4,6,7]. In Ref. [4], the halo nucleus is easily broken up by the removal of the loosely bound halo neutrons. The breakup effect is represented by complex DPP with repulsive real part and attractive imaginary part that is important for increasing the reaction cross section due to the breakup effect. In Ref. [6], the DPP is also taken as complex surface potential that is added to the real folded and imaginary WS potentials for $^6\text{He} + ^{12}\text{C}$ and $^6\text{Li} + ^{12}\text{C}$. The DPP is shown to affect the total optical potential strongly at the surface and gives estimation for the strength of breakup effect. The DPP is also deduced microscopically from the inversion of the S matrix in the framework of the coupled discretized continuum channels (CDCC) calculations [8–10]. The DPP is found to be strongly repulsive real part and very small absorptive imaginary part

that is quite different from heavy-ion scattering with small real part. The repulsive effect of the breakup channels can be stimulated well simply by reducing the real part of the optical potential in the folding model to reproduce the elastic data in the single-channel calculation [8–10]. The DPP for ^{11}Li scattering from ^{12}C at 637 MeV was calculated using both two- and three-body descriptions of the ^{11}Li structure applying Glauber theory for the scattering and breakup processes [11]. It has been found that the real part of the DPP is repulsive in the far nuclear surface. The DPP is also calculated within the semiclassical approach [12,13]. The DPP is taken as an exponential tail imaginary potential and is evaluated according to the breakup probability. Several authors [5,14–20] have studied and calculated the DPP and breakup effect of halo nuclei.

Recently, the elastic scattering of ^{11}Be on ^{12}C has been measured at 38.4 MeV/nucleon up to 14° in the center-of-mass (c.m.) frame [2], which covers considerably wider angles than the previous measurement at 49.3 MeV/nucleon [12]. The ^{11}Be breakup from $2s$ state has been discussed in Refs. [2,12,14,18]. The real potential of this reaction at 38.4 MeV/nucleon is calculated within the framework of the folding model using CDM3Y density-dependent effective nucleon-nucleon (NN) interaction [2]. The coupling effect is stimulated by introducing the complex repulsive phenomenological surface potential that is added to the real folded and WS imaginary potentials. In Ref. [14], $^{11}\text{Be} + ^{12}\text{C}$ is treated at 49.3 MeV/nucleon as a three-body $^{10}\text{Be} + n + ^{12}\text{C}$ problem and is discussed using the semiclassical eikonal approximation. The phenomenological potential of $^{11}\text{Be} + ^{12}\text{C}$ is obtained based on $^{10}\text{Be} + ^{12}\text{C}$ and $n + ^{12}\text{C}$ potentials. The projectile excitation and breakup effects are found to be significant. Also, the $^{11}\text{Be} + ^{12}\text{C}$ scattering cross sections are calculated using the adiabatic approximation [18]. It is found that the coupling of the elastic and projectile excitation channels is crucial to the analysis, and a simple relationship exists between the elastic scattering of a composite halo nucleus and of its core from a stable target. The DPP for the $^{11}\text{Be} + ^{12}\text{C}$ reaction at 49.3 MeV/nucleon is calculated in the

* mym.hassan@yahoo.com

† myhfarag@hotmail.com

‡ h.maridi@yahoo.com

framework of semiclassical theory [12]. An exponential tail is assumed for the imaginary surface potential with diffuseness directly related to the small decay length of the initial wave function that describes the long range of the polarization potential. The polarization potential, which is added to the phenomenological optical potential, gives an enhancement in the reaction cross section.

In the present work, we have analyzed the elastic-scattering data of $^{11}\text{Be} + ^{12}\text{C}$ at 38.4 MeV/nucleon in microscopic double folding model using density-independent M3Y effective NN interaction and different forms of ^{11}Be density distribution. The coupling of the elastic channels to breakup channel is taken into account. The DPP is calculated using different methods. First, it is taken phenomenologically as surface derivative as in Refs. [2,4,6,7]. The second method involves the use of a semiclassical method based on the probability for the breakup of $^{11}\text{Be} \rightarrow ^{10}\text{Be} + n$, as in Refs. [12,13]. For the third method, it is obtained microscopically as the derivative of the folding potential. Also, an approximation to the simple phenomenological DPP is carried out. The folding model analysis for $^{11}\text{Be} + ^{12}\text{C}$ elastic scattering is given in Sec. II. The different methods for the calculation of the DPP are presented in Sec. III. The applications of these methods for $^{11}\text{Be} + ^{12}\text{C}$ system are given in Sec. IV. The applications for $^{11}\text{Li} + ^{12}\text{C}$ and $^6\text{He} + ^{12}\text{C}$ are presented in Sec. V. The conclusions are given in Sec. VI.

II. FOLDING MODEL ANALYSIS FOR $^{11}\text{Be} + ^{12}\text{C}$ ELASTIC SCATTERING

The real nucleus-nucleus optical potential in the double folding model is given by the expression [21]

$$V_F(r) = \int \rho_1(\mathbf{r}_1)\rho_2(\mathbf{r}_2)v_{nn}(s)d\mathbf{r}_1d\mathbf{r}_2, \quad (1)$$

where $\rho_1(\mathbf{r}_1)$, $\rho_2(\mathbf{r}_2)$ are the nuclear matter density distributions for projectile and target nuclei, respectively, and $v_{nn}(s)$ is the effective NN interaction with $s = |\mathbf{r} - \mathbf{r}_1 + \mathbf{r}_2|$ is the distance between the two nucleons.

The popular M3Y NN interaction is used. It is derived by Bertsch *et al.* [22], it is obtained from the fitting of the G -matrix element of the Reid-Elliott NN interaction. The parameterized form of the M3Y interaction introduced by Satchler and Love [21] is given as

$$v_{nn}(s) = 7999 \frac{\exp(-4s)}{4s} - 2134 \frac{\exp(-2.5s)}{2.5s} + J_{00}(E)\delta(s), \quad (2)$$

where the zero-range pseudopotential $J_{00}(E)$ represents the single-nucleon exchange term and is given by [21]

$$J_{00}(E) = -276(1 - 0.005E/A) \text{ MeV fm}^3, \quad (3)$$

where E and A are the incident energy and the mass number of the projectile, respectively.

The neutron halo nuclei are assumed to be composed of a core surrounded by a halo of one or more neutrons [1,23], so we consider the one neutron halo nucleus ^{11}Be to be composed of a ^{10}Be core and one-neutron.

$$\rho_{^{11}\text{Be}}(r) = \rho_{^{10}\text{Be}}(r) + \rho_n(r). \quad (4)$$

The root-mean-square (rms) radius of ^{11}Be is quite large compared to that of ^{10}Be . The density of ^{10}Be core is assumed to be of a Gaussian form [24] with rms radius equals to 2.46 fm [25]. While the parameters of the halo density are adjusted to obtain the rms radius of ^{11}Be which equals to 2.90 fm [26]. The deduced core size of ^{11}Be slightly exceeds the measured radius of ^{10}Be , which is assumed to be the core in ^{11}Be . This may be explained by the fact that the motion of the center-of-mass of the core around the center-of-mass of the whole nucleus increases the effective core size. This may be due to the core polarization [27]. To test the sensitivity to the radial shape of the nuclear matter distribution, three different nuclear matter density distributions are assumed, one being a Gaussian with $R_m = R_c = R_v = 2.90$ fm (where R_c , R_v , and R_m denote the rms radii of the core, valence neutron, and the halo nuclei distributions). The two others being the sum of two distributions, a Gaussian for the core nucleons (with $R_c = 2.46$ fm) and the valence neutron is assumed to have either $1p$ or $2s$ shell distributions. The rms radius of one-halo neutron density, R_v , can be obtained from [28,29]

$$R_m = \left[\frac{10R_c^2 + R_v^2}{11} \right]^{1/2}. \quad (5)$$

Therefore, the value of R_v equals 5.7 fm. We denote the three densities as G, G1p, and G2s, respectively. The three density distributions have the same nuclear matter radius R_m but have different radial shapes. The G1p and G2s densities have long tails due to the consideration of the core-halo structure.

The three different densities of ^{11}Be nucleus that have been used are plotted in Fig. 1. One can see that the G density, which describes the ^{11}Be nucleus as a whole, has no tail while the other two densities that are formed from the core and one valence neutron yield an extended tail in ^{11}Be nucleus. So these describe better the halo structure of the ^{11}Be nucleus with a large radius. It is clear that, at $r < 5$ fm, G1p and G2s densities are mainly formed from the core. However, at $r > 5$ fm the halo contribution for the two densities is dominant.

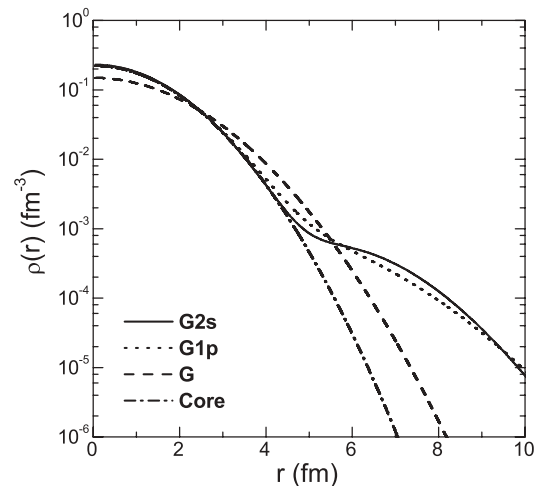


FIG. 1. Densities of ^{11}Be used in this work.

The density of ^{12}C nucleus was given by Vineyard *et al.* [30] in harmonic oscillator (HO) form

$$\rho_{^{12}\text{C}}(r) = \rho_0(1 + \alpha r^2) \exp(-\beta r^2), \quad (6)$$

where $\rho_0 = 0.1644 \text{ fm}^{-3}$, $\alpha = 0.4988 \text{ fm}^{-2}$, and $\beta = 0.3741 \text{ fm}^{-2}$ with $(r_{\text{rms}}^2)^{1/2} = 2.407 \text{ fm}$ [31].

The real part of the optical potential for the reaction $^{11}\text{Be} + ^{12}\text{C}$ is calculated using the double folding model. The imaginary part is taken as a part of the folded potential. The total optical potential can be written as

$$U_{\text{opt}}(r) = (N_R + iN_I)V_F(r) + U_C(r), \quad (7)$$

where N_R and N_I are the renormalization factors of the real and imaginary microscopic potentials, respectively. V_F is the folded potential that is calculated with density-independent M3Y effective NN interaction, and the Coulomb potential $U_C(r)$ is taken as the usual Coulomb form between a point charge and a uniform charge distribution of radius $R_c = r_c(A_P^{1/3} + A_T^{1/3})$ with $r_c = 1.2 \text{ fm}$ [6]. A search on the renormalization factors N_R and N_I are carried out to give best fit with experimental data.

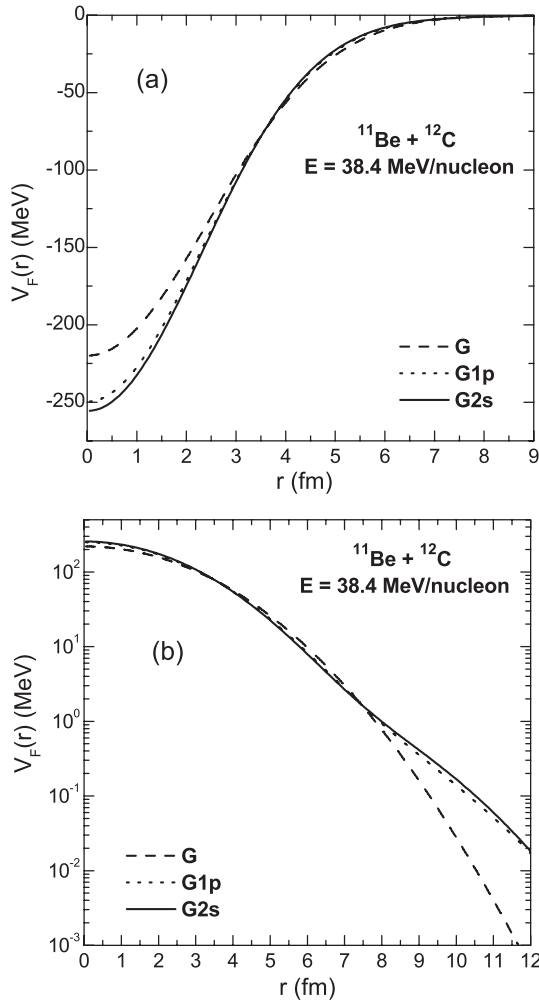


FIG. 2. Real folded potentials of $^{11}\text{Be} + ^{12}\text{C}$ system at 38.4 MeV/nucleon obtained using M3Y interaction with G, G1p, and G2s densities, shown in (a) linear scale and (b) logarithmic scale.

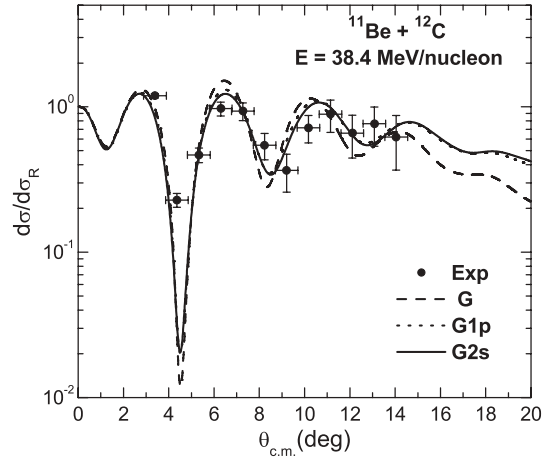


FIG. 3. Elastic-scattering cross sections for $^{11}\text{Be} + ^{12}\text{C}$ at 38.4 MeV/nucleon in the comparison with the optical model (OM) results given by the folded potential (obtained with M3Y interaction) with different densities.

Figure 2 presents the real folded potentials [Eq. (1)] for elastic scattering of $^{11}\text{Be} + ^{12}\text{C}$ at 38.4 MeV/nucleon that is calculated with M3Y effective NN interaction and different densities: G, G1p, and G2s. They are given without the renormalization factor N_R (i.e., $N_R = 1$). It is seen that the potential using the G density has a smaller depth than that of the G1p and G2s densities. At large distance, the folded potential using the G density falls rapidly than the potentials obtained using the other two densities that have longer range. This is due to the type of each density.

The differential cross sections of $^{11}\text{Be} + ^{12}\text{C}$ elastic scattering at the energy 38.4 MeV/nucleon using real and imaginary folded potentials with M3Y interaction for different densities of ^{11}Be nucleus are presented in Fig. 3. The renormalization factors N_R and N_I that give good fitting with the experimental data and the total reaction cross sections are listed in Table I. One can notice that the result with G density gives fitting with lower quality than that with the other two densities and it has the largest χ^2 . The results with the two densities G1p and G2s are approximately similar. The results with G2s density give relatively the best result because it gives fitting with χ^2 relatively smaller than G1p density.

The effect of changing the renormalization factors N_R and N_I is presented in Fig. 4 for $^{11}\text{Be} + ^{12}\text{C}$ elastic-scattering data using the folding potential that is calculated with M3Y interaction and G2s density. The fitting sets of the renormalization factors N_R and N_I and the obtained reaction cross sections are

TABLE I. Renormalization parameters of optical potential for the elastic $^{11}\text{Be} + ^{12}\text{C}$ cross sections at 38.4 MeV/nucleon and reaction cross sections obtained by fitting the experimental data [2] using M3Y effective NN interaction with different densities.

Density type	N_R	N_I	χ^2	σ_R (mb)
G	0.67	0.52	10.87	1355
G1p	0.77	0.53	8.48	1406
G2s	0.8	0.55	8.09	1430

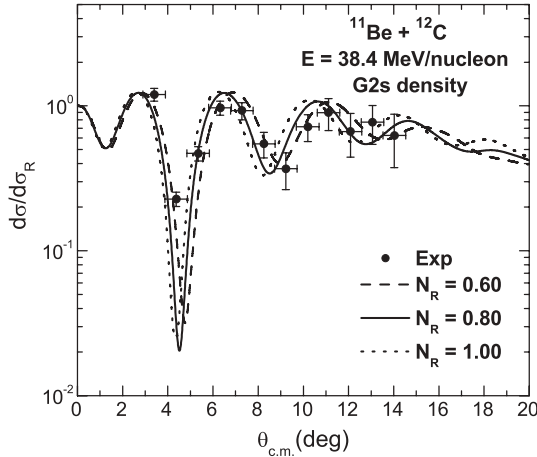


FIG. 4. Elastic-scattering cross sections for $^{11}\text{Be} + ^{12}\text{C}$ at 38.4 MeV/nucleon in the comparison with the OM results given by the folded potential (obtained with M3Y interaction and G2s density) with different fits.

listed in Table II. One can see that the result with $N_R = 0.6$ is in good agreement with $\theta_{c.m.} < 10^\circ$ but has lower fitting in $\theta_{c.m.} > 10^\circ$. However, without the renormalization factor ($N_R = 1.0$), the result is in good agreement for large angles better than for small angles. While the result with $N_R = 0.8$ has a reasonable agreement with most of the experimental data. It is noted that increasing the value of N_R reduces the width of minima and maxima so shifts the obtained curve to the left. The reduction of the real potential in the double folding model is explained well as the coupling effect of the channels on the elastic scattering. But the simple renormalization procedure fails to reproduce the data over the whole angular range. Therefore, the breakup effect is taken into consideration by adding the polarization potential to the optical potential. In the following section, we present several methods for the calculation of the DPP. The applications of these methods for $^{11}\text{Be} + ^{12}\text{C}$ system are given in Sec. IV.

III. POLARIZATION POTENTIAL DUE TO BREAKUP

The very weak binding of the halo neutron of ^{11}Be with small separation energy ($S_n = 0.503$ MeV) makes the ^{11}Be nucleus more susceptible to breakup in the field of the target nucleus as $^{11}\text{Be} \rightarrow ^{10}\text{Be} + n$. Then, the DPP is introduced, which represents the effect of coupling to breakup channels.

TABLE II. Renormalization parameters of the optical potential for the elastic $^{11}\text{Be} + ^{12}\text{C}$ cross sections at 38.4 MeV/nucleon and reaction cross sections obtained by fitting the experimental data [2] using M3Y effective NN interaction and G2s density with different fitting sets.

N_R	N_I	χ^2	σ_R (mb)
0.6	0.39	4.69	1283
0.8	0.55	8.09	1430
1.0	0.69	12.55	1533

It is added to the “bare” optical potential. It has a longer range than the “bare” optical potential, and it is also complex potential as

$$U_{\text{pol}}(r) = V_{\text{pol}}(r) + iW_{\text{pol}}(r), \quad (8)$$

where V_{pol} and W_{pol} are the real and imaginary dynamical polarization potentials, respectively. According to Feshbach theory of microscopic optical potential [32], the real part of the total potential is taken as $V_F + V_{\text{pol}}(r)$ which may almost be approximated well by $\simeq N_R V_F$ in a single channel calculation [10]. This is just the origin of the reduction of N_R in the folding model. In this work, different methods will be given for the calculation of the DPP. These are semiclassical approximation, phenomenological, and microscopic methods.

A. DPP from semiclassical approximation

According to Refs. [12,13], the surface imaginary optical potential $W_s[\mathbf{R}(t)]$ represents the transfer and breakup reactions. $\mathbf{R}(t) = \mathbf{b}_c + vt$ is the classical trajectory of relative motion for the nucleus-nucleus collision with constant velocity v in the z direction and core-target impact parameter \mathbf{b}_c in the xy plane [33]. For a halo nucleus at high incident energy the transfer probability is going to be much smaller than the breakup probability, therefore the surface potential has been identified here with the breakup potential and can be related to the breakup probability as

$$\int_{-\infty}^{\infty} W_s[\mathbf{R}(t)] dt = -\frac{\hbar}{2} P_{\text{bup}}(b_c), \quad (9)$$

with $P_{\text{bup}}(b_c) = P_0(b_c)p_{\text{bup}}(b_c)$, where P_{bup} is the breakup probability, p_{bup} is the total breakup probability, and P_0 is a damping factor that has been referred as the core survival probability that has been parameterized as [12]

$$P_0(r) = |S_{\text{CT}}|^2 = \exp[-\ln 2e^{(R_s - r)/a_0}] \quad (10)$$

within the strong absorption radius $R_s = 1.4(A_P^{1/3} + A_T^{1/3})$ fm, $a_0 = 0.6$ fm $^{-1}$, and S_{CT} is the scattering S matrix due to the core-target interaction. $P_0 = 1$ is assumed at large distances. The effect of breakup is most important at large distances ($b_c > R_s$). The breakup probability is given by [12,33,34]

$$p_{\text{bup}} \approx \int d\epsilon_f \sum_{l_f} (|1 - \langle S_{l_f} \rangle|^2 + 1 - |\langle S_{l_f} \rangle|^2) B(l_f, l_i). \quad (11)$$

Equation (11) gives the neutron transfer probability from a definite single-particle state of energy ϵ_i , momentum $\gamma_i = \sqrt{-2m\epsilon_i/\hbar}$, and angular momentum l_i in the projectile to a final continuum state of energy ϵ_f , and momentum $k_f = \sqrt{2m\epsilon_f/\hbar}$ within an interval $d\epsilon_f$. It is the sum of transfer probabilities to each possible final l_f state in the energy bin $d\epsilon_f$. $\langle S_{l_f} \rangle$ is the optical model scattering matrix that describes the rescattering of the neutron on the target [35] and the factor $B(l_f, l_i)$ is the elementary transfer probability and is given

by [12,33,34]:

$$B(l_f, l_i) = \frac{1}{2} \left(\frac{\hbar}{mv} \right)^2 \frac{m}{\hbar^2 k_f} (2l_f + 1) P_{l_f}(X_f) \times |C_1|^2 \frac{e^{-2\eta b_c}}{2\eta b_c} P_{l_i}(X_i), \quad (12)$$

where

$$X_i = 2 \left(\frac{k_1}{\gamma_i} \right)^2 + 1, \quad X_f = 2 \left(\frac{k_2}{k_f} \right)^2 - 1.$$

Also

$$k_1 = -\frac{(\varepsilon_i - \varepsilon_f + \frac{1}{2}mv^2)}{\hbar v} \quad \text{and} \quad k_2 = -\frac{(\varepsilon_i - \varepsilon_f - \frac{1}{2}mv^2)}{\hbar v}$$

are the z component of the neutron momentum in the initial and final state, respectively. η is the modulus of the transverse component of the neutron momentum and is given by $\eta = \sqrt{k_1^2 + \gamma_i^2} = \sqrt{k_2^2 - k_f^2} \frac{mv^2}{2}$ is the incident energy per nucleon at the distance of closest approach for the ion-ion collision. $|C_1|^2$ is the asymptotic normalization constant of the initial wave function. P_{l_i} and P_{l_f} are the Legendre polynomials coming from the angular part of the initial and final wave functions.

In the case of a weakly bound projectile, in the limit of the small initial binding energies, it is found that $k_2 \approx k_f$ and $P_{l_f} \approx 1$ [33]. By introducing the classical angular momentum $\lambda = k_f b_n$ and $(2l_f + 1) = 2\lambda$ in Eq. (11) the sum over l_f can be replaced with an integral over the neutron-target impact parameters b_n with respect to the target. The phase shift can be approximated by the eikonal form such that [33]

$$S_{l_f} \approx e^{-i\chi(b_n)}, \quad (13)$$

with

$$\chi(b_n) = \frac{1}{\hbar v} \int_{-\infty}^{\infty} V_2(x, y, \hat{z}) d\hat{z},$$

where V_2 is the neutron-target complex potential and can be taken as a Global phenomenological optical potential [36]. Equation (11) can be written as [33,34]

$$p_{\text{bup}} \approx \int d\varepsilon_f \frac{dp}{d\varepsilon_f}, \quad (14)$$

where

$$\frac{dp}{d\varepsilon_f} = \frac{m}{\hbar^2 k_f} \int_0^{\infty} b_n db_n (|1 - e^{-i\chi(b_n)}|^2 + 1 - |e^{-i\chi(b_n)}|^2) |C_1|^2 \frac{e^{-2\eta b_c}}{2\eta b_c} P_{l_i}(X_i), \quad (15)$$

where

$$|\tilde{\Psi}_1(b_c, k_1)|^2 \approx |C_1|^2 \frac{e^{-2\eta b_c}}{2\eta b_c} P_{l_i}(X_i).$$

$|\tilde{\Psi}_1|^2$ is the initial state momentum distribution [33,34].

In Eq. (14), p_{bup} has a maximum at the minimum value of $\eta = \gamma_i$. Also, the main dependence on the core-target impact parameter b_c contained in the exponential factor $e^{-2\eta b_c}$. Therefore, after integrating over ε_f the b_c dependence of the

breakup probability $p_{\text{bup}}(b_c)$ will still be of the exponential form $p_{\text{bup}}(b_c) \approx e^{-b_c/\alpha}$ with $\alpha = \frac{1}{2\gamma_i}$, where γ_i is the decay length of the neutron initial state wave function [12,13]. At large distances, where $P_0 = 1$, it is assumed that the same exponential dependence for the absorptive potential, $W_s(r) = W_0 e^{-r/\alpha}$, and $\mathbf{R}(t) = \mathbf{b}_c + vt$. Then, Eq. (9) reads [12,13]:

$$\int_{-\infty}^{\infty} W_s(b_c, z) dz = -\frac{\hbar v}{2} p_{\text{bup}}(b_c). \quad (16)$$

The left-hand side with assumption of $b_c \gg z$ can be approximately evaluated as

$$\int_{-\infty}^{\infty} W_s(b_c, z) dz = W_0 \int_{-\infty}^{\infty} e^{-(b_c + \frac{z^2}{2b_c})} dz = W_0 \sqrt{2\pi b_c \alpha} e^{-b_c/\alpha}. \quad (17)$$

Equating the right-hand sides of Eqs. (16) and (17) gives

$$W_0(b_c) = -\frac{\hbar v}{2} p_{\text{bup}}(b_c) \frac{1}{\sqrt{2\pi b_c \alpha}} e^{b_c/\alpha}. \quad (18)$$

In the nuclear induced peripheral reactions like breakup and transfer, most of the cross section comes from impact parameters around the strong absorption radius R_s [12]. Also, the initial state amplitude $|\tilde{\Psi}_1|^2$ depends on the choice of $b_c = R_s$ [33]. Therefore, the surface imaginary optical potential that is assumed as $W_s(r) = W_0 e^{-r/\alpha}$, as indicated above, can be written as

$$W_s(r) = -\frac{\hbar v}{2} p_{\text{bup}}(R_s) \frac{1}{\sqrt{2\pi \alpha R_s}} \exp\left(-\frac{r - R_s}{\alpha}\right), \quad (19)$$

where $\alpha = \frac{1}{2\gamma_i}$ with $\gamma_i = \frac{\sqrt{-2m\varepsilon_i}}{\hbar}$. ε_i is the separation energy of the neutron. For ^{11}Be , $\varepsilon_i = -0.503$ MeV so $\alpha = 3.2$ fm.

B. Phenomenological DPP

The DPP has an exponential behavior outside the target nucleus. It can be taken as simple phenomenological surface Woods-Saxon (WS) form and can be defined as [2,4,6,7]

$$U_{\text{pol}}(r) = -(V_p + iW_p) f_P(r), \quad (20)$$

where

$$f_P(r) = \frac{\exp\left(\frac{r-R_p}{a_p}\right)}{\left[1 + \exp\left(\frac{r-R_p}{a_p}\right)\right]^2}. \quad (21)$$

The real part is repulsive ($V_p \leq 0$).

Equation (20) can be rewritten by considering $f_P(r)$ at large distance [4]. Then, the phenomenological DPP can be approximated as:

$$U_{\text{pol}}(r) = -(V_p + iW_p) \exp\left(-\frac{r - R_p}{a_p}\right). \quad (22)$$

Now, comparing the imaginary parts of Eq. (22) and Eq. (19), identifying R_p as R_s and a_p as α . Hence, Eq. (22) can be rewritten in the form

$$U_{\text{pol}}(r) = -(\bar{V}_p + i\bar{W}_p) \exp\left(-\frac{r - R_s}{\alpha}\right), \quad (23)$$

with two free parameter \bar{V}_p and \bar{W}_p . According to Feshbach theory [10,32], $\bar{V}_p \leq 0$ to the real DPP becomes repulsive. \bar{W}_p is attractive to give an enhancement in the total reaction cross section due to the breakup. Equation (23) represents an approximation of the simple phenomenological DPP at the surface where the breakup effect is important. This approximated DPP is characterized by two fitting parameters only and the diffuseness of this DPP reflects the small decay length of the neutron wave function entering breakup, so the long range of the polarization potential is obtained.

C. Microscopic DPP from the derivative of the folding potential

By analogy with Eq. (20) for phenomenological surface potential, the surface potential can be obtained microscopically from the derivative of the folding potential as

$$U_{\text{pol}}(r) = -(N_{rp} + iN_{ip})r \frac{dV_F(r)}{dr}, \quad (24)$$

where N_{rp} and N_{ip} are the normalization factors of real and imaginary polarization potential. Similarly as before, the repulsive real part ($N_{rp} \leq 0$) to verify Feshbach theory of microscopic optical potential [10,32].

IV. DYNAMICAL POLARIZATION POTENTIAL FOR $^{11}\text{Be} + ^{12}\text{C}$ SYSTEM

Let us denote the DPP as Semi. DPP, Pheno. DPP I, Pheno. DPP II, and Micr. DPP for dynamical polarization potentials that are obtained by semiclassical approximation [Eq. (19)], simple phenomenological with four free parameters [Eq. (20)], the approximated phenomenological with two free parameters [Eq. (23)], and microscopic [Eq. (24)] forms, respectively.

First, the differential cross sections of $^{11}\text{Be} + ^{12}\text{C}$ elastic scattering at 38.4 MeV/nucleon are calculated with the DPP from simple phenomenological and semiclassical approximation methods. The DPP is added to the bare optical potential that consists of the real and imaginary folded potentials with M3Y effective NN interaction and G2s density. The results of these calculations are presented in Fig. 5. The fitting renormalization factors of the folded potentials and the parameters of the different forms of DPP are listed in Table III. The parameters of the Pheno. DPP I from Ref. [2] are found to

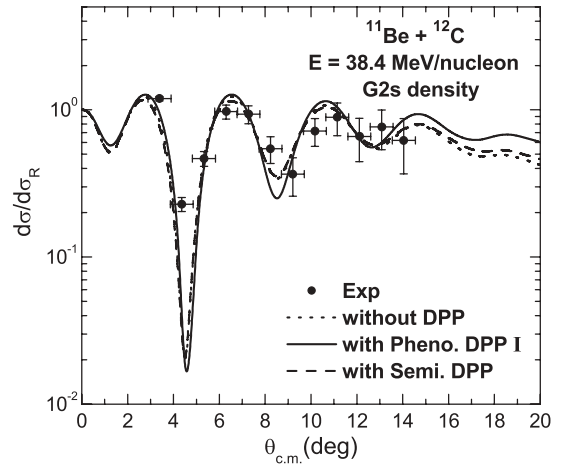


FIG. 5. Elastic-scattering cross sections for $^{11}\text{Be} + ^{12}\text{C}$ at 38.4 MeV/nucleon in comparison with the OM results given by the folded potential (obtained with M3Y interaction and G2s density) with Pheno. DPP I and Semi. DPP and without DPP.

be the best-fitting parameters with the present work. Without adding the DPP, the data require suitable renormalization of the real folded potential (see Table III).

The result with the phenomenological DPP leads to a good fitting with the experimental data. When the Pheno. DPP I is added, the real folded potential does not require a renormalization (see Table III). This feature of the DPP is in agreement with Sakuragi's treatment of DPP [8]. The reaction cross section is almost unchanged by increasing V_p but is significantly increased by W_p [4].

In semiclassical approximation method that suggests adding only imaginary part of DPP, the value of N_R is found to be the same one that obtained without DPP. Semi. DPP gives reaction cross section larger than that obtained with Pheno. DPP I.

Second, Fig. 6 compares the data of $^{11}\text{Be} + ^{12}\text{C}$ at 38.4 MeV/nucleon with phenomenological, microscopic, and without DPP. The fitting parameters of folded and polarization potentials are given in Table III. Micr. DPP is fitted with two parameters only, whereas there are four parameters in Pheno. DPP. I. One can notice that no significant difference between pheno. DPP I and Micr. DPP. From Table III, one can see that

TABLE III. Renormalization parameters of real N_R and imaginary potentials N_I , fitting parameters of different forms of DPP, and reaction cross sections, obtained by fitting the elastic-scattering data for $^{11}\text{Be} + ^{12}\text{C}$ [2] that were calculated using G2s density and M3Y effective NN interaction at the energy 38.4 MeV/nucleon.

DPP type	N_R	N_I	Fitting parameters of DPP	χ^2	σ_R (mb)
Without	0.8	0.55		8.09	1430
Semi.	0.8	0.50		7.99	1616
Pheno. I	1.0	0.47	$V_p = -88$ MeV, $W_p = 20$ MeV $R_p = 0.0$ fm, $a_p = 1.68$ fm	7.08	1500
Pheno. II	1.0	0.40	$\bar{V}_p = -2.8$ MeV, $\bar{W}_p = 0.21$ MeV $R_s = 6.32$ fm, $\alpha = 3.2$ fm	5.85	1584
Micr.	1.0	0.40	$N_{rp} = -0.04$, $N_{ip} = 0.02$	7.73	1430

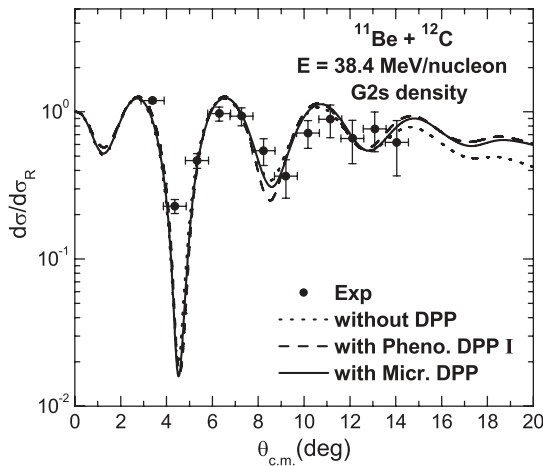


FIG. 6. Elastic-scattering cross sections for $^{11}\text{Be} + ^{12}\text{C}$ at 38.4 MeV/nucleon in comparison with the OM results given by the folded potential (obtained with M3Y interaction and G2s density) with Pheno. DPP I and Micr. DPP and without DPP.

the Pheno. DPP I gives reaction cross section larger than Micr. DPP. However, when the Pheno. DPP I and Micr. DPP are added to the folded potential, the real folded potential does not require a renormalization.

Third, the cross sections of $^{11}\text{Be} + ^{12}\text{C}$ system at 38.4 MeV/nucleon with the simple phenomenological (with four free parameters) and the approximated phenomenological (with two free parameters) polarization potentials are plotted in Fig. 7. This figure shows that the two polarization potentials, Pheno. DPP I and Pheno. DPP II, have approximately the same behavior at angles ($\theta_{c.m.} > 5^\circ$) while the Pheno. DPP II is the best at small angles ($\theta_{c.m.} < 5^\circ$). The renormalization factors of the bare optical potential and the fitting parameters of Pheno. DPP I and II, and the reaction cross section are listed in Table III. From this table, one can notice that the total reaction cross section (σ_R) with Pheno. DPP II is greater than Pheno. DPP I.

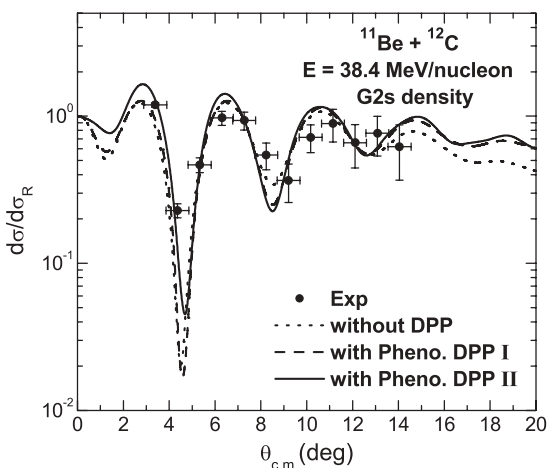


FIG. 7. Elastic-scattering cross sections for $^{11}\text{Be} + ^{12}\text{C}$ at 38.4 MeV/nucleon in comparison with the OM results given by the folded potential (obtained with M3Y interaction and G2s density) with Pheno. DPP I and Pheno. DPP II and without DPP.

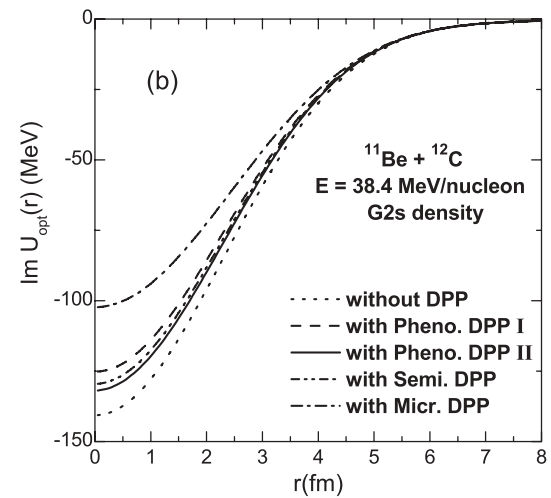
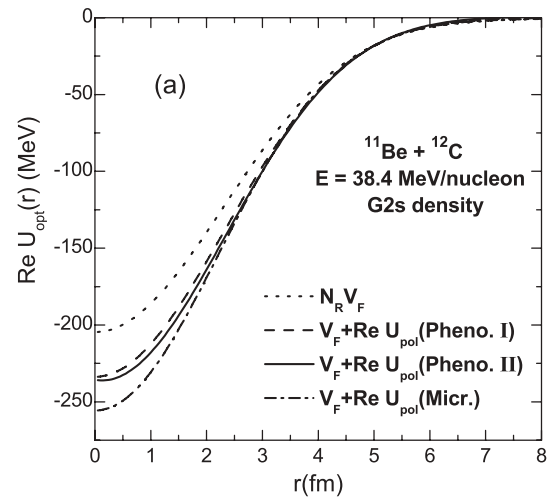


FIG. 8. The folded potential is calculated with M3Y interaction and G2s density for $^{11}\text{Be} + ^{12}\text{C}$ elastic-scattering at 38.4 MeV/nucleon. The renormalized potentials is represented with the dotted line. The dashed, dash-dotted, dash-double dotted, and solid lines represent the total real and imaginary optical potentials that are calculated by adding Pheno. DPP I, Pheno. DPP II, Semi. DPP, and Micr. DPP, respectively, to the folded potential.

The total real and imaginary potentials including the DPP in different forms are presented in Figs. 8(a) and 8(b), respectively. It is clear that the total potentials ($V_F + \text{Re } U_{\text{pol}}$) with different types of the DPP are very close to the renormalized folded potential ($N_R V_F$) at the surface (at $r \simeq 5$ fm), these real potentials are shallower than the renormalized folded potential at small distances [see Fig. 8(a)]. This result is found in Refs. [6,8]. But this behavior is found to be reversed for the imaginary potentials [see Fig. 8(b)]. The renormalization procedure, which reduces the potential on the whole range, may not give a correct potential at small distance. Therefore it is better to add the DPP, which reduces the folding potential mostly at 4–5 fm [6,37]. One can see that the additional of DPP shows slightly better fitting of differential cross sections than without adding the DPP at large angles (above 12°). This feature corresponds to the behavior of the potential at small distances (< 5 fm) for different models [see Fig. 8(a)].

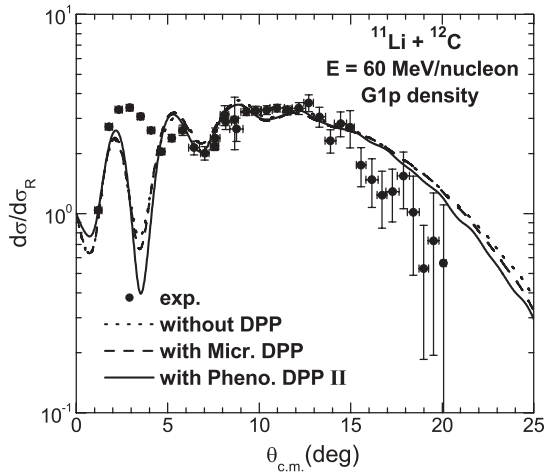


FIG. 9. Elastic-scattering cross sections for $^{11}\text{Li} + ^{12}\text{C}$ at 60 MeV/nucleon in comparison with the OM results given by the folded potential (obtained with M3Y interaction and G1p density) with Pheno. DPP II and Micr. DPP and without DPP.

V. APPLICATION FOR TWO-NEUTRON HALO NUCLEI REACTIONS

The two methods, Micr. DPP and Pheno. DPP II, successfully describe the breakup effect well for the elastic scattering of the one-neutron halo (^{11}Be nucleus). It is interesting to apply these methods to the elastic scattering of weakly bound two-neutron halo nuclei from the stable nuclei, namely $^{11}\text{Li} + ^{12}\text{C}$ at 60 MeV/nucleon and $^6\text{He} + ^{12}\text{C}$ at 38.3 MeV/nucleon.

The elastic-scattering data for $^{11}\text{Li} + ^{12}\text{C}$ at 60 MeV/nucleon [38] is calculated using the double folding model. The folded potential has been obtained using M3Y NN interaction and Gaussian-oscillator (GO) density, which has the same form as G1p density, with parameters $R_c = 2.50$ fm, $R_v = 5.86$ fm, and $R_m = 3.37$ fm [27]. The breakup effect is considered by adding Pheno. DPP II and Micr. DPP to the bare potential. The results of these calculations are presented in Fig. 9. The fitting parameters of the optical potential with Pheno. DPP II and Micr. DPP and without DPP are given in Tables IV and V. The separation energy of the two halo neutrons equals 0.247 MeV [23] that is needed to calculate the diffuseness of the Pheno. DPP II.

One can see that the results with Pheno. DPP II, Micr. DPP, and without DPP have similar behavior but the Pheno. DPP II gives deeper first minimum and larger reaction cross

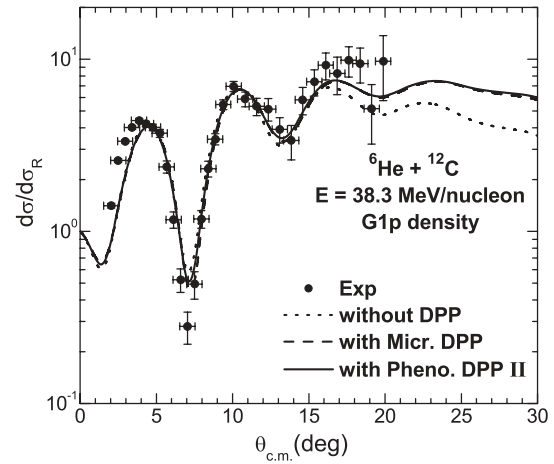


FIG. 10. Elastic-scattering cross sections for $^6\text{He} + ^{12}\text{C}$ at 38.3 MeV/nucleon in comparison with the OM results given by the folded potential (obtained with M3Y interaction and G1p density) with Pheno. DPP II and Micr. DPP and without DPP.

section than Micr. DPP and without DPP. Using Pheno. DPP II slightly gives better fitting for large angles (above 15°) and gives enhancement in the reaction cross section as in Refs. [4,11].

Referring to the work of Al-Khalili and Tostevin's [11], it was found that the real part of the DPP is repulsive in far nuclear surface, whereas in the present work, the real part of the DPP is repulsive in the whole range. This point needs further investigation. However, the imaginary part of the DPP is found to be attractive in the present work as in Al-Khalili and Tostevin work.

The elastic-scattering data for $^6\text{He} + ^{12}\text{C}$ at 38.3 MeV/nucleon [6] are calculated using the double folding model. The folded potential has been obtained using M3Y NN interaction and GO density with parameters $R_c = 1.81$ fm, $R_v = 3.05$ fm, and $R_m = 2.30$ fm [28]. The data are reproduced, including the breakup effect when the Pheno. DPP II and the Micr. DPP are added to the bare potential. The results of these calculations are presented in Fig. 10. The fitting parameters of the optical potential with Pheno. DPP II and Micr. DPP and without DPP are given in Table IV where the separation energy of the two halo neutrons equals 0.97 MeV [23].

One can see that the results with adding both Pheno. DPP II and Micr. DPP are better than that without adding DPP. Both

TABLE IV. Renormalization parameters of real and imaginary potentials, N_R and N_I , fitting parameters of the approximated phenomenological and microscopic DPP, and reaction cross sections, obtained by fitting the experimental data for different reactions. The other parameters of Pheno. DPP II are listed in Table V.

Reaction	Energy (MeV/nucleon)	DPP type	N_R	N_I	Fitting parameters of DPP	χ^2	σ_R (mb)
$^{11}\text{Li} + ^{12}\text{C}$	60.0	Without	1.0	0.5		47.8	1508
		Pheno. II	1.0	0.43	$\bar{V}_p = -2.0$ MeV, $\bar{W}_p = 0.21$ MeV	52.30	1589
		Micr.	1.0	0.36	$N_{rp} = -0.02$, $N_{ip} = 0.02$	48.0	1503
$^6\text{He} + ^{12}\text{C}$	38.3	Without	1.0	0.55		29.74	1041
		Pheno. II	1.0	0.36	$\bar{V}_p = -0.61$ MeV, $\bar{W}_p = 0.46$ MeV	30.49	1100
		Micr.	1.0	0.34	$N_{rp} = -0.02$, $N_{ip} = 0.02$	33.0	1004

TABLE V. Calculated parameters of the Pheno. DPP II for different reactions.

Reaction	Energy (MeV/nucleon)	R_s (fm)	α (fm)
$^{11}\text{Be} + ^{12}\text{C}$	38.4	6.319	3.211
$^{11}\text{Li} + ^{12}\text{C}$	60.0	6.319	3.241
$^6\text{He} + ^{12}\text{C}$	38.3	5.749	1.635

give good description at the large angles for the measured data, which has not been achieved by renormalization of the folded potentials only. This is also found in Ref. [6].

It is interesting that the renormalization factors of the imaginary part of microscopic DPP is found to have same value ($N_{ip} = 0.02$) for the three reactions considered in this work (see Tables III and IV).

VI. CONCLUSION

The optical potentials and cross sections of $^{11}\text{Be} + ^{12}\text{C}$ elastic scattering at 38.4 MeV/nucleon are calculated within the framework of the double folding model. The real and imaginary parts of the optical potential are constructed by a folding M3Y effective nucleon-nucleon interaction. The density of ^{11}Be nucleus is assumed to be composed of two parts, a ^{10}Be core and one valence neutron. Different types of density distributions that have the same rms radius are used, namely G, G1p, and G2s. The renormalization factors for the real and imaginary microscopic potentials, N_R and N_I , are introduced.

The results of the calculations of $^{11}\text{Be} + ^{12}\text{C}$ elastic scattering show that the two densities G1p and G2s gives approximately similar behavior so the form of the one valence

neutron density has a small effect on the obtained cross sections. But G2s density can be considered relatively better than G1p density.

The study of changing the renormalization factor N_R shows that the result without renormalization has lower fitting at $\theta_{c.m.} < 11^\circ$, whereas the result with $N_R = 0.6$ has lower fitting at $\theta_{c.m.} > 10^\circ$. A reasonable agreement with most of the experimental data is obtained with $N_R = 0.8$. Therefore, the real folding potential needs a suitable reduction that gives an estimation of the breakup channel effects on the elastic-scattering channel.

These results show that the single-channel calculation with the folded potentials failed to reproduce the measured data over the whole angular range. So, the breakup effect is introduced by adding a complex DPP to the “bare” potential. The DPP is taken in different forms that have been obtained from phenomenological Woods-Saxon, semiclassical approximation, microscopic (from the derivative of the folding potential) methods. Also, the phenomenological DPP is approximated and related to the semiclassical approximation theory.

The results with introducing the DPP show that the real folded potential does not need a renormalization and the Feshbach theory is satisfied. Adding the DPP gives reaction cross section larger than the folded potential alone that may identify the breakup or neutron(s) removal cross section.

The microscopic and approximated phenomenological DPP succeeded to describe the breakup effect for studying different reactions. These DPPs give an explicit justification for the long range of the polarization potential, whereas the simple phenomenological DPP is a generalized description and includes no structure information of the interacting nuclei.

-
- [1] S. N. Ershov, T. Rogde, B. V. Danilin, J. S. Vaagen, I. J. Thompson, and F. A. Gareev, Phys. Rev. C **56**, 1483 (1997).
[2] V. Lapoux *et al.*, Phys. Lett. **B658**, 198 (2008).
[3] M. E. Brandan and G. R. Satchler, Phys. Rep. **285**, 143 (1997).
[4] M. S. Hussein and G. R. Satchler, Nucl. Phys. **A567**, 165 (1994).
[5] K. Yabana, Y. Ogawa, and Y. Suzuki, Phys. Rev. C **45**, 2909 (1992).
[6] V. Lapoux *et al.*, Phys. Rev. C **66**, 034608 (2002).
[7] V. Lapoux *et al.*, Phys. Lett. **B517**, 18 (2001).
[8] Y. Sakuragi, Phys. Rev. C **35**, 2161 (1987).
[9] Y. Sakuragi, M. Yahiro, and M. Kamimara, Prog. Theor. Phys. **70**, 1047 (1983).
[10] Y. Sakuragi, M. Yahiro, and M. Kamimara, Prog. Theor. Phys. Suppl. **89**, 136 (1986).
[11] J. S. Al-Khalili and J. A. Tostevin, Phys. Rev. C **49**, 386 (1994).
[12] A. Bonaccorso and F. Carstoiu, Nucl. Phys. **A706**, 322 (2002).
[13] Awad A. Ibraheem and A. Bonaccorso, Nucl. Phys. **A748**, 414 (2005).
[14] J. S. Al-Khalili, J. A. Tostevin, and J. M. Brooke, Phys. Rev. C **55**, R1018 (1997).
[15] L. F. Canto, R. Donangelo, and M. S. Hussein, Nucl. Phys. **A529**, 243 (1991).
[16] L. F. Canto, R. Donangelo, M. S. Hussein, and M. P. Pato, Nucl. Phys. **A542**, 131 (1992).
[17] J. C. Pacheco and N. Vinh Mau, Nucl. Phys. **A669**, 135 (2000).
[18] R. C. Johnson, J. S. Al-Khalili, and J. A. Tostevin, Phys. Rev. Lett. **79**, 2771 (1997).
[19] J. S. Al-Khalili, Nucl. Phys. **A581**, 315 (1995).
[20] J. S. Al-Khalili, I. J. Thompson, and J. A. Tostevin, Nucl. Phys. **A581**, 331 (1995).
[21] G. R. Satchler and W. G. Love, Phys. Rep. **55**, 183 (1979).
[22] G. F. Bertsch, J. Borysowicz, H. McManus, and W. G. Love, Nucl. Phys. **A284**, 399 (1977).
[23] I. Tanihata, J. Phys. G: Nucl. Part. Phys. **22**, 157 (1996).
[24] R. A. Rego, Nucl. Phys. **A581**, 119 (1995).
[25] I. Tanihata *et al.*, Phys. Rev. Lett. **55**, 2676 (1985).
[26] J. S. Al-Khalili and J. A. Tostevin, Phys. Rev. Lett. **76**, 3903 (1996).
[27] A. V. Dobrovolsky *et al.*, Nucl. Phys. **A766**, 1 (2006).
[28] G. D. Alkhozov *et al.*, Nucl. Phys. **A712**, 269 (2002).
[29] M. Y. M. Hassan, M. Y. H. Farag, E. H. Esmael, and H. M. Maridi, Phys. Rev. C **79**, 014612 (2009).
[30] M. F. Vineyard, J. Cook, K. W. Kemper, and M. N. Stephens, Phys. Rev. C **30**, 916 (1984).

- [31] Shen Qing-biao, Feng Da-chun, and Zhuo Yi-zhong, Phys. Rev. C **43**, 2773 (1991).
- [32] H. Feshbach, Ann. Phys. (NY) **5**, 357 (1958).
- [33] A. Bonaccorso and D. M. Brink, Phys. Rev. C **58**, 2864 (1998).
- [34] A. Bonaccorso and F. Carstoiu, Phys. Rev. C **61**, 034605 (2000).
- [35] A. Bonaccorso and D. M. Brink, Phys. Rev. C **44**, 1559 (1991).
- [36] R. L. Varner, W. J. Thompson, T. L. McAbee, E. J. Ludwig, and T. B. Clegg, Phys. Rep. **201**, 57 (1991).
- [37] D. T. Khoa, G. R. Satchler, and W. von Oertzen, Phys. Rev. C **51**, 2069 (1995).
- [38] J. J. Kolata *et al.*, Phys. Rev. Lett. **69**, 2631 (1992).